Differential hERG ion channel activity of ultrasmall gold nanoparticles

Annika Leifert[a], Yu Pan[b], Anne Kinkeldey[b], Frank Schiefer[a], Julia Setzler[c], Olaf Scheel[d], Hera Lichtenbeld[e], Günter Schmid[f], Wolfgang Wenzel[c], Willi Jahnen-Dechent[b,1], and Ulrich Simon[a,1]

[a]Institute of Inorganic Chemistry and Jülich Aachen Research Alliance-Fundamentals of Information Technology, and [b]Helmholtz-Institute for Biomedical Engineering, Biointerface Laboratory, Rheinisch-Westfälische Technische Hochschule Aachen University, 52074 Aachen, Germany; [c]Karlsruhe Institute of Technology, 76344 Eggenstein-Leopoldshafen, Germany; [d]Cytocentrics Bioscience GmbH, 18059 Rostock, Germany; [e]HLConsulting, 6202 TC, Maastricht, The Netherlands; and [f]Institute of Inorganic Chemistry, University of Duisburg-Essen, 80639 Munich, Germany

Edited* by Chad A. Mirkin, Northwestern University, Evanston, IL, and approved April 4, 2013 (received for review November 21, 2012)

Understanding the mechanism of toxicity of nanomaterials remains a challenge with respect to both mechanisms involved and product regulation. Here we show toxicity of ultrasmall gold nanoparticles (AuNPs). Depending on the ligand chemistry, 1.4-nm-diameter AuNPs failed electrophysiology-based safety testing using human embryonic kidney cell line 293 cells expressing human ether-á-go-go-Related gene (*hERG*), a Food and Drug Administration-established drug safety test. In patch-clamp experiments, phosphine-stabilized AuNPs irreversibly blocked hERG channels, whereas thiol-stabilized AuNPs of similar size had no effect in vitro, and neither particle blocked the channel in vivo. We conclude that safety regulations may need to be reevaluated and adapted to reflect the fact that the binding modality of surface functional groups becomes a relevant parameter for the design of nanoscale bioactive compounds.

shape | complementarity | gold cluster | nanotoxicology

Gold nanoparticles (AuNPs) have been extensively explored in biomedical applications, for example as drug carriers, contrast agents, or therapeutics (1–4). They can be applied to selectively target cancer cells through guiding ligands for advanced medical imaging (5) or to regulate gene expression through high-density surface functionalization with oligonucleotides (6). The binding of such functional molecules to the surface of AuNPs is facilitated via thiol groups, resulting in a relatively stable gold–sulfur bond. Established cytotoxicity tests including gene expression studies have proved those AuNPs to be nontoxic (7–9). In contrast, ultrasmall AuNPs (sub-2 nm) may become cytotoxic, when the capping ligands are weaker binding phosphines instead of thiols. Previously we reported unexpected cytotoxicity of ultrasmall (sub-2 nm) AuNPs, capped with sodium (3-diphenylphosphino)benzenesulfonic acid (TPPMS). This cytotoxicity was size dependent in several cell lines and most severe in the case of AuNPs comprising a 55-gold-atom cluster core with a diameter of 1.4 nm and a shell consisting of 12 TPPMS molecules (Au1.4MS) (10). Toxicity was caused by oxidative stress (8). We further showed that cytotoxicity (*i*) was abolished by replacing the phosphine ligands by thiols, which bind more strongly to the gold core, and (*ii*) decreases with increasing particle size with a significantly reduced toxicity already at 1.8 nm.

However, results from cell toxicity assays cannot always accurately reflect the complex effects that nanoparticles (NPs) might cause in living animals with regard to biological barriers, development, and organ function (11). Recently we determined that Au1.4MS was teratogenic in zebrafish embryos, leading to, e.g., cardiac malformation (9). We asked whether this was the result of cardiotoxicity. Ultrasmall NPs approach the hydrodynamic size of drug molecules and therefore potentially also interact with ion channels. However, few studies directly addressed the interaction of NPs with ion channels.

The human ether-á-go-go-Related gene product (hERG/K_v11.1) (12) is notorious for broad-specific interaction with many promising candidate drugs that passed initial cytotoxicity screens, but turned out to be highly cardiotoxic in preclinical trials. The hERG ion channel is a voltage-gated potassium channel that mediates the rapid delayed rectifier K^+ current in the heart (I_{Kr}). Together with other ion channels hERG determines the cardiac action potential and regulates the heartbeat. Disturbance of hERG channel function caused by drug binding as an unwanted side effect of medication can lead to life-threatening arrhythmias, due to prolonged time between the Q-wave and the T-wave of the heart's electrical cycle [acquired long QT syndrome (LQTS)]. This has led to the removal of several drugs from the market and is now a significant hurdle in the development of new drugs (13). Therefore, new drug candidates must be tested for a potential inhibitory effect on the hERG current as a first step in a nonclinical testing strategy [Guidance of the International Committee for Harmonization (ICH) topic S7B by the Food and Drug Administration] (14). Because of structural peculiarities the hERG channel interacts with many different highly diverse chemical compounds (15). The cavity of the tetrameric hERG channel protein is supposed to be wider compared with those of related K^+ channels, thus providing more space for chemical compounds to interact. Several aromatic residues line this cavity. In particular the aromatic residues Tyr652 and Phe656 form a promiscuous binding site for diverse chemical compounds. Cytotoxic CdSe NPs with a core diameter of 2.4 nm did not affect the electrophysiological properties of cells overexpressing the hERG channel, but caused cytotoxicity due to the release of Cd^{2+} ions (16).

In this study we performed whole-cell patch-clamp recordings to evaluate the effect of Au1.4MS on the hERG tail currents. Scheme 1 illustrates the experimental setup and molecular structures of tested species. Au1.4MS concentration dependently blocked the channel within minutes (Fig. 1*A*). A total of 3.1 μM extracellular Au1.4MS (determined by atomic absorption spectroscopy (AAS) as [Au], equaling ~56 nM particle concentration) caused a slight decrease of hERG tail current amplitude. Increasing concentration up to 16.25 μM further declined the tail current. Channel blockade was irreversible in the sense that perfusion with extracellular buffer (EC) did not recover the hERG current.

The perfusion with 65 μM Au1.4MS (particle concentration of 1.18 μM) for 10 min led to more than 50% decreased hERG tail current amplitude (Fig. 1*B*). Subsequent washing with EC confirmed irreversible current inhibition. Further perfusion with 65 μM Au1.4MS revealed an additive blocking effect. A half-maximal blocking concentration of 16.9 μM was determined by automated

Author contributions: A.L., Y.P., H.L., G.S., W.J.-D., and U.S. designed research; A.L., Y.P., A.K., J.S., O.S., and W.W. performed research; F.S. contributed new reagents/analytic tools; A.L., Y.P., J.S., O.S., and W.W. analyzed data; and A.L., Y.P., W.J.-D., and U.S. wrote the paper.

The authors declare no conflict of interest.

*This Direct Submission article had a prearranged editor.

[1]To whom correspondence may be addressed. E-mail: ulrich.simon@ac.rwth-aachen.de or willi.jahnen@rwth-aachen.de.

This article contains supporting information online at www.pnas.org/lookup/suppl/doi:10.1073/pnas.1220143110/-/DCSupplemental.

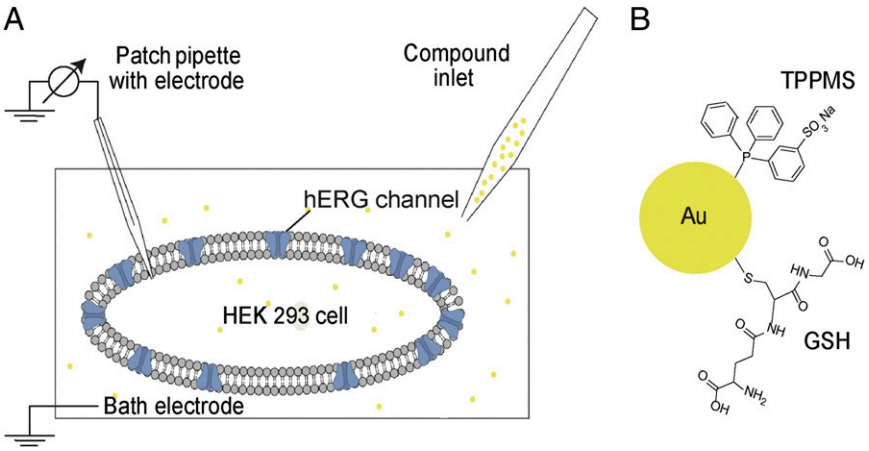

Scheme 1. Schematic illustrations of the experimental setup and the molecular structure of tested species (not drawn to scale). (*A*) Scheme of patch-clamp setup in whole-cell configuration of a HEK 293 cell with hERG ion channels. Via the inlet, extracellular buffer (EC) or the respective test compound solution is perfused in the cell chamber. The connection between patch pipette and cell membrane is sealed to ensure a gigaohm seal, and the patch pipette is used to apply the voltage protocol as well as to record the response current. (*B*) AuNP surface with TPPMS ligand (with a AuNP core of 1.4 nm resulting in Au1.4MS) and GSH ligand (with a AuNP core of 1.1 nm resulting in Au1.1GSH), respectively.

patch-clamp measurements (Fig. S1). Control experiments ruled out that the patch-clamp measurements were compromised by gold ions ($Au^{1+/3+}$) or by artifacts related to an interaction of the AuNPs with the patch-clamp setup (see *SI Text* for details).

The cytotoxic effects of Au1.4MS in an in vitro cell test typically appear after 1 h incubation. As the hERG channel inhibition is observed within minutes, we conclude that hERG blockade was not causing immediate toxicity in cells, but nevertheless indicated potentially cardiotoxic interaction with the ion channel in animals.

Typical hERG blockers such as cisapride, terfenadine, or dofetilide interact with the aromatic amino acids Tyr652 and Phe656 of the hERG (17–19). As Au1.4MS is stabilized by TPPMS, a sulfonated triphenylphosphine, an inhibitory interaction mediated by the aromatic moieties of the ligand shell is conceivable. Therefore, we tested the effect of the TPPMS ligand alone on hERG. Au1.4MS consists of 12 TPPMS molecules per particle and 55 gold atoms; thus at 3 μM Au1.4MS the TPPMS concentration is ~0.65 μM. Fig. 1*C* shows that pure TPPMS up to 100 μM had no effect on hERG current amplitudes. At fivefold higher concentration of 500 μM the amplitude decreased within 1 min. In contrast to the irreversible blockade of Au1.4MS, TPPMS blockade was reversible when the cell was washed with EC afterward. TPPMS blocking of the hERG channel is therefore highly unlikely to cause Au1.4MS block of hERG.

Previous cytotoxicity studies demonstrated a strong dependence of AuNP toxicity on the ligand shell (8). Glutathione (GSH)-stabilized AuNPs were nontoxic compared with Au1.4MS, most likely due to strong binding of the thiol functionality of GSH to the gold core. GSH-stabilized, 1.1-nm–sized AuNPs (Au1.1GSH) were thus also analyzed by the patch-clamp technique. Au1.1GSH did not block the hERG channel at 300 μM applied for 13 min (Fig. 2*A*). AuroVist, which are 1.9-nm-diameter thiol-stabilized AuNPs, were also tested (20). Like Au1.1GSH, AuroVist did not affect the hERG current up to 300 μM (Fig. 2*B*). We assume that the gold cores of thiol-stabilized AuNPs are shielded sufficiently strongly to prevent interaction with biological targets whereas Au1.4MS can shed its weaker bound phosphine shell and thus can interact with biological target molecules.

Previous studies showed that the addition of excess TPPMS can efficiently suppress the cytotoxicity of Au1.4MS (8). Hence, solutions of 20 μM Au1.4MS, which on their own caused a full block of hERG, were mixed with excess TPPMS. When cells were

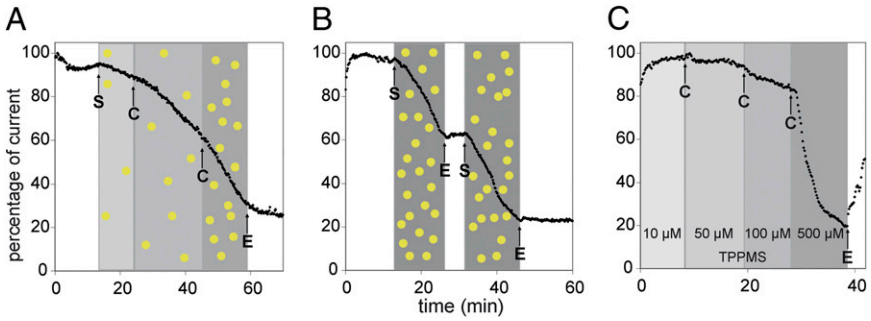

Fig. 1. Patch-clamp measurement of hERG tail current peak amplitudes in HEK 293 cells stably expressing the hERG ion channel. (*A*) Concentration-dependent inhibition of hERG current by Au1.4MS (3.1 μM, 6.5 μM, and 16.25 μM gold atom concentrations), sequentially applied to the same cell. The shaded areas indicate the intervals of different compound concentrations [Au] and [TPPMS], respectively. After a latency time of typically 2–3 min, an increase in the slope of current decay with increasing Au1.4MS concentration is observed. Arrows indicate start (S) and change (C) of perfusion with the differently concentrated AuNP solutions; E is end of sample perfusion (perfusion with EC). (*B*) Inhibition of hERG current by 65 μM Au1.4MS shows no recovery upon washout. Arrows indicate start (S) and end (E) of perfusion with AuNP solution. The blocking of the hERG channel by Au1.4MS is irreversible and additive. (*C*) Effect of TPPMS on the hERG tail current. Totals of 10 μM, 50 μM, 100 μM, and 500 μM TPPMS were subsequently perfused to the same cell. A total of 10 μM was applied from the start; arrows indicate change (C) and end (E) of sample perfusion. A total of 500 μM induces considerable channel inhibition, which is reversible, as opposed to blocking by Au1.4MS.

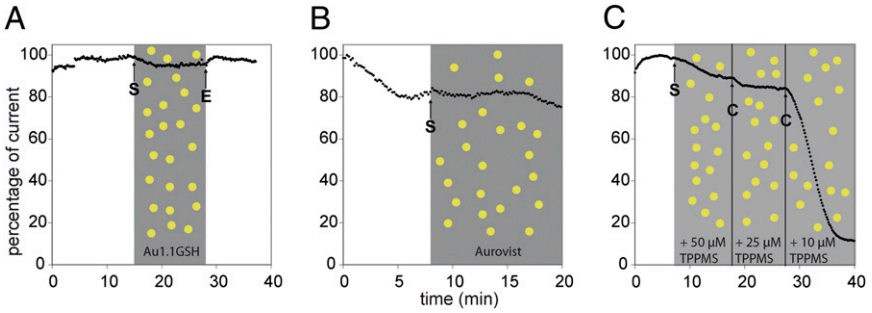

Fig. 2. hERG tail current peak amplitudes in the presence of thiol-stabilized AuNPs or Au1.4MS with excess TPPMS. (*A* and *B*) Application of (*A*) 300 μM Au1.1GSH and (*B*) 300 μM AuroVist did not affect the hERG current. The shaded areas indicate the intervals of different compound concentrations of [Au] in Au1.1GSH (*A*), of [Au] in AuroVist (*B*), and of [TPPMS] (*C*), and the arrows indicate start (S) and end (E) of perfusion. (*C*) Preincubation of Au1.4MS with different concentrations of TPPMS abolished the hERG blocking potency of 20 μM Au1.4MS when TPPMS was present in excess. The cell was perfused with a mixture of 20 μM Au1.4MS + 50 μM TPPMS, 20 μM Au1.4MS + 25 μM TPPMS, and 20 μM Au1.4MS + 10 μM TPPMS. Arrows indicate start (S) and change (C) of sample perfusion.

exposed to a mixture of 20 μM Au1.4MS and 50 μM TPPMS, only a slight decrease in the hERG tail current amplitude was detected (Fig. 2*C*). This slight decrease was slower and less steep than the usual pronounced block of hERG and was statistically insignificant. At 10 min, a 20/25-μM mixture of AuNP and TPPMS likewise did not influence the hERG current. Upon further reduction of the TPPMS/AuNP ratio to 10 μM TPPMS and 20 μM Au1.4MS, the typical reduction of tail current amplitude was again observed.

In a control experiment, the cells were preincubated with 50 μM TPPMS for 10 min, rinsed, and subsequently treated with 20 μM Au1.4MS. In this case, the current inhibition was not prevented (Fig. S2). Thus, the addition of excess free TPPMS ligand abolished the hERG channel block by Au1.4MS if the AuNPs were preincubated before application to the cell and if the concentration ratio exceeded a certain value. It is known for triphenylphosphine-stabilized AuNPs that a dissociation equilibrium of bound and free ligand molecules is formed in solution (21). If the accessibility of the gold core surface is crucial for the blocking mechanism of Au1.4MS, the addition of excess TPPMS will shift this equilibrium and make the particle surface less accessible.

This hypothesis was probed by modeling. We prepared a model for Au1.4MS, using the starting structure for the Au_{55} icosahedron from the Cambridge Cluster database (22), and attached TPPMS ligands at the 12 apex gold atoms of the cluster (denoted as [Au1.4MS(12)]). We also constructed a homology model for the hERG channel (Fig. S3), based on homology to the Mammalian Shaker Kv1.2 potassium channel [Protein Data Bank (PDB) ID: 2A79] (23), which agrees well with the hERG consensus model (24). Next we performed Monte Carlo simulations for the Au_{55} cluster with a varying number of ligands (Fig. S4) in which [Au1.4MS(12)] was allowed to sample both the intra- and the extracellular entrances of the channel. In the simulations using the pH 7.4 model of the channel, we found that Au1.4MS explores the vicinity of the pore on both sides of the channel, but does not dock because of a repulsive Coulomb energy. This can be understood in the sense that both the channel and the ligands are negatively charged. In control simulations, where the channel was parameterized at pH 6.7, we found that the [Au1.4MS(12)] bound weakly to the channel. We therefore hypothesized that binding to the channel would be improved if negatively charged ligands were displaced from the Au_{55} core upon binding. Because this process cannot be modeled quantitatively with available classical potentials, we prepared models of [Au1.4MS(n)] (with n = 0, 2, 4, 6, 8, 10, 12) and docked those using the same simulation protocol described above.

These simulations established a trend for both channel models, where binding becomes increasingly likely as the number of ligands on the Au_{55} decreases. The complex electrostatic environment near the channel entrance and exit is not fully accounted for in our simulations, because the membrane and the counter-ion distribution of the phospholipid head groups is not quantitatively represented, but interpolation between the docking results for the two channel models indicates that at least some ligands need to be displaced from the Au_{55} core to obtain a stable complex between the channel and the AuNP. Representative binding modes from the simulations for [Au1.4MS(0)], [Au1.4MS(6)], and [Au1.4MS(12)] are shown in Fig. 3.

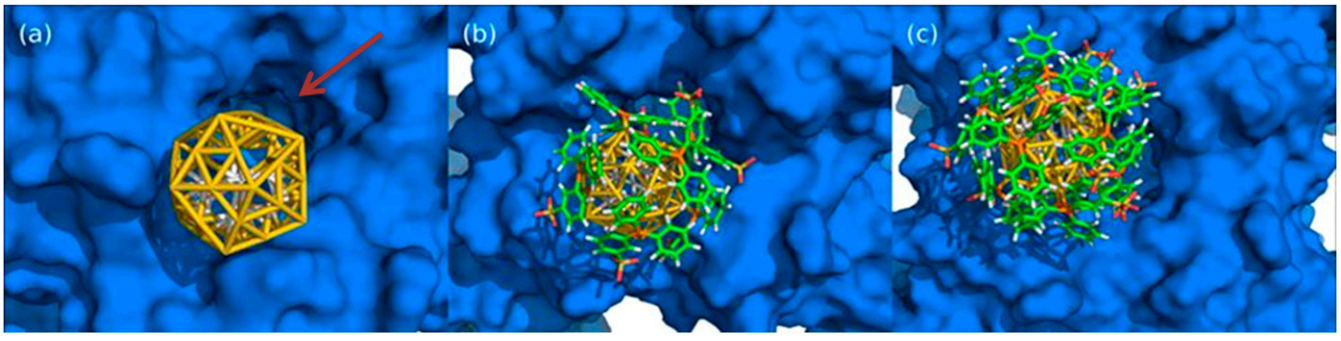

Fig. 3. Molecular simulation of nanoparticle docking to the intracellular hERG channel: (*A*) without TPPMS ligands [Au1.4MS(0)], (*B*) partially covered with 6 TPPMS [Au1.4MS(6)], and (*C*) with 12 TPPMS ligands [Au1.4MS(12)]. Shown are the molecular surface of the intracellular channel entrance (blue), the Au1.4 cluster in icosahedral form (yellow), and the ligands in element-specific color coding (C, green; O, red; S, yellow; P, orange; H, white). The dark red arrow in *A* indicates the entrance to the cavity on the intracellular side of the channel. This cavity can accommodate small-molecule ligands influencing hERG activity, but in our model not even the naked Au1.4 particle.

In all of the binding modes we find that Au1.4MS is too large to enter the cavity at the intracellular side of the channel. In particular we observe no specific interactions between the aromatic side chains of the Phe656 residues (25). Because of its size, Au1.4MS(n) can also not bind near the entrance of the K^+ passage at the bottom of the extracellular channel side. We therefore hypothesize that the channel entrance is the preferred binding site for the AuNP in our experiments.

It is known that NPs form a protein corona when confronted with protein-containing solutions like serum or full blood (26, 27). Stronger-binding ligands or ligands in excess may displace weaker ligands from the AuNP surface. This can be investigated by NMR spectroscopy, as was shown by Schmid (21). The reaction of fetal calf serum (FCS) with Au1.4MS was therefore investigated by ^{31}P-NMR spectroscopy. The TPPMS molecules of pure Au1.4MS give a peak at 46 ppm, compared with free TPPMS at −8.3 ppm in water and −4.6 ppm in water plus FCS. A solution of Au1.4MS containing 10% FCS showed a peak at 2.4 ppm, thus revealing a release of TPPMS molecules from the AuNP surface, probably due to replacement by serum proteins (NMR spectra in Fig. S5).

We therefore repeated the patch-clamp experiments in the presence of FCS to more closely mimic a live animal situation involving blood circulation, where Au1.4MS was found to be cytotoxic. Pretreatment of cells with EC + 10% FCS induced a slight decrease in tail current amplitude to a stable value (Fig. 4*A*). In contrast to FCS-free incubations, Au1.4MS (300 μM final concentration) with 10% FCS added did not cause any channel blockade. We conclude that FCS formed a protein corona around the AuNPs, most probably around the cluster core by multiple weak coordinative interactions, which prevented direct interaction of AuNPs with the ion channel. Thus, the cytotoxicity of Au1.4MS observed in several cell lines even in the presence of FCS, and in zebrafish and mice, was likely not due to hERG channel blockade. To confirm that AuNP toxicity is not primarily due to cardiotoxicity we studied mice with respect to QT prolongation (28).

The onset of blockade of the hERG channel is reflected in the electrocardiography (ECG) as the prolongation of the QT interval. The QT prolongation represents the duration of an average ventricular action potential. A prolonged QT interval is a risk factor for the episodes of torsade de pointes (29). Fig. 4 shows the regular ECG waveform and absence of QT prolongation in the mouse after injection with Au1.4MS (Fig. 4*B*), confirming the lack of hERG blockade by Au1.4MS previously observed in hERG-transfected HEK 293 cells in the presence of serum. This observation is a bona fide example of the complexities encountered in safety testing of designed nanocomposites as opposed to small-molecule drugs: The toxicity profile is not determined by the core material, here the AuNP, but affected by the ligand composition. The most drastic effect, irreversible blockade of the channel observed in vitro, is likely going to be pharmaceutically irrelevant due to serum interactions. In light of this finding protocols for toxicity tests for metallic NPs need to be reevaluated and adapted to reflect these complexities; in particular, scenarios with the opposite change in the toxicity profile with serious detrimental effects on patients may also occur. If we consider ligands that cannot be replaced in aqueous medium and show a low toxicity profile in vitro, but where the ligand shell is degraded over time in the physiological environment, naked NPs that irreversibly block the channel may be released.

In conclusion, Au1.4MS was found in whole-cell patch-clamp recordings to differentially interact with the hERG potassium ion channel expressed in HEK 293 cells. The blockade of the hERG channel by Au1.4MS was irreversible. It was not caused by the ligand TPPMS, which caused a reversible blockade, and only at very high concentrations. We also excluded gold ion impurities as active species. The investigation of other, thiol-stabilized AuNPs as well as the addition of excess TPPMS to Au1.4MS indicated that the binding strength of the ligand shell and the shielding of the AuNP surface played a crucial role. We hypothesize that the blocking species of Au1.4MS was the Au core after partial or complete shedding of the TPPMS shell. Our findings were corroborated by modeling of AuNPs, carrying a varying number of ligands in contact with the hERG channel, suggesting a differential interaction facilitated by the complementarity in size and shape. Thus, we show that NPs can act as an antagonist for a subcellular functional system due to shape complementarity at a molecular scale.

To create test conditions that are more closely aligned with in vivo conditions, we repeated the patch-clamp experiments with Au1.4MS in the presence of FCS. Here, no blocking of the hERG channel was observed. This was most likely due to the formation of a shielding protein corona around the AuNPs, most probably due to ligand exchange reactions mediated by multivalent coordinative binding, which inhibits a direct interaction of the AuNPs with the ion channel. ECG measurements in mice injected i.v. with Au1.4MS confirmed this finding, in that no arrhythmia was found. This reflects the mechanism of how the antagonistic AuNPs are converted into inactive derivatives and

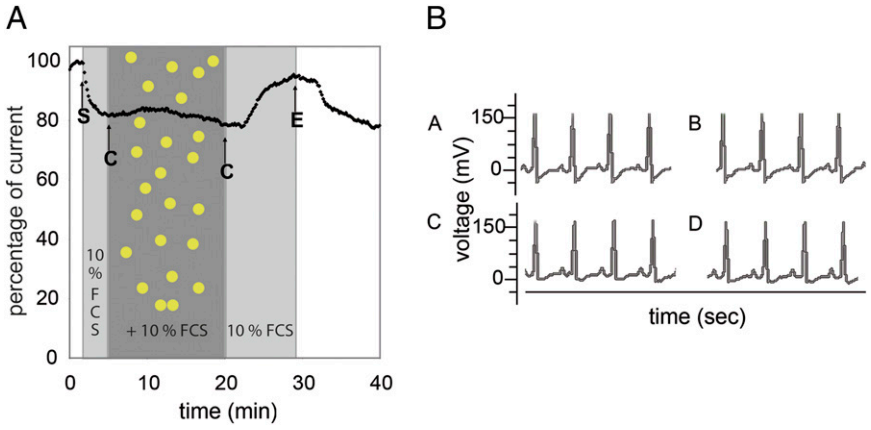

Fig. 4. hERG tail current peak amplitudes in the presence of FCS and the representative mouse ECG waveforms recorded pre- and postinjection. The shaded areas indicate the intervals of FCS addition and Au1.4MS + FCS addition. (*A*) Application of 300 μM Au1.4MS in the presence of 10% FCS in the EC does not inhibit the hERG channel current. A slightly reduced tail current is observed with 10% FCS in EC (starting at arrow S) compared with EC without FCS. Other arrows indicate change (C) to Au1.4MS + 10% FCS and back to 10% FCS (after 20 min) and end (E) of sample perfusion. (*B*) ECG is taken before injection (A and C) and 6 d postinjection (B and D). The Mouse is injected with 0.9% NaCl (B) and 50 mg/kg Au1.4MS (D).

suggests safe use of Au1.4MS in biomedical applications regarding potential cardiotoxicity despite a conflicting whole-cell patch-clamp assay conducted according to regulatory body guidelines. Electrophysiological peculiarities of animal species preclude, however, extending this statement beyond mice.

Methods

Gold Nanoparticle Synthesis. Chemicals used were $HAuCl_4 \cdot 3\ H_2O$ (Sigma-Aldrich; ACS reagent), triphenylphosphine (Alfa Aesar; 99+ wt%), $NaBH_4$ [Aldrich; purum pro analysi (p.a.)], $BF_3 \cdot OEt_2$ (Aldrich), H_2SO_4 (Grüssing; p.a.), GSH (Fisher BioReagents; ≥98 wt%), Au(I)-TPPMS-Cl (ABCR; 98 wt%), sodium auro(I)thiomalate hydrate (Tauredon) (Aldrich), Bis(2-methoxyethyl) ether (Acros; 99 wt%), benzene (AppliChem; p.a.) dichloromethane (VWR; p.a.), and methanol (VWR; p.a.). All chemicals were used as received. Water was obtained from a water purification system (ELGA Purelab Ultra). AuroVist (1.9-nm–sized AuNPs) was purchased from Nanoprobes.

TPPMS was synthesized as described in ref. 30. Triphenylphosphine-stabilized AuNPs (1.4-nm sized) were synthesized as described before (31) and transferred to the water phase via a two-phase ligand exchange reaction to yield TPPMS-stabilized Au1.4MS (10). The resulting particles have a mean molecular formula of $Au_{55}TPPMS_{12}Cl_6$, i.e., 12 ligand molecules per nanoparticle. Au1.1GSH was synthesized by a procedure from Negishi et al. (32). The AuNPs were characterized by scanning transmission electron microscopy (STEM), elemental analysis, and ultraviolet and visible spectroscopy. Concentrations of AuNP solutions were determined as [Au], using AAS.

Patch-Clamp Experiments. HEK 293 cells stably expressing the hERG ion channel were used (Instant Cells; Cytocentrics Bioscience GmbH) (33). The cells are stored in liquid nitrogen and are ready to use directly after thawing without any cultivation. After thawing, the cells were resuspended in extracellular buffer and kept in the Cytocentrics cell reservoir as a cell suspension at a density of 2.0 million/mL in extracellular buffer at room temperature and were used for 4 h after thawing. The EC was used for thawing the cells, the storage in the cell reservoir, and the preparation of the working concentrations of the test compounds. The extracellular buffer consists of 140 mM NaCl, 2.5 mM KCl, 2 mM $MgCl_2$, 2 mM $CaCl_2$, 10 mM Hepes, 10 mM glucose, and 15 mM sucrose. The buffer was adjusted to pH 7.4 ± 0.1 and osmolality 320 ± 5 mOsm/kg. The buffer was stored at 4 °C and heated to room temperature prior to use. The intracellular buffer (IC) consisted of 100 mM K-gluconate, 20 mM KCl, 1 mM $CaCl_2$, 1 mM $MgCl_2$, 10 mM Hepes, 11 mM EGTA-KOH, 4 mM ATP-Mg^{2+}, 3 mM phosphocreatine-Na_2-H_2O, and 9 mM sucrose. The buffer was adjusted to pH 7.2 ± 0.1 and osmolality 295 ± 5 mOsmol/L. Aliquots are stored at –20 °C. Prior to use an aliquot IC was thawed and used no longer than for 4 h. For test compounds, the different gold nanoparticles were dissolved in ultrapure water as stock solutions and diluted with EC in the concentrations needed for the experiments directly before the experiments. When Au1.4MS was preincubated with TPPMS or GSH, both compounds were diluted in EC to the respective concentrations, mixed, and kept at 37 °C for 3 h. Patch-clamp recordings were performed on a manual patch-clamp setup equipped with a HEKA EPC-10 patch-clamp amplifier (HEKA Elektronik; software PatchMaster v2.15). Patch pipettes were pulled from Borosilicate glass with a pipette resistance between 1.5 and 4 MOhm. As a pipette electrode, a chlorinated silver wire was used; the reference electrode was an Ag/AgCl pellet electrode (Warner Instruments). The bath chamber (RC-25 with platform P-3; Warner Instruments) was continuously perfused with EC or compound solution via a peristaltic pump (ISM 830; Ismatec). For patch-clamp recordings cells were seeded onto a coverslip placed in the bath chamber. After gigaseal formation and whole-cell breakthrough, the cell was lifted from the coverslip with the pipette and positioned close to the perfusion entry of the bath chamber and continuously perfused with EC until a stable recording condition was established (approximately 10 min). Only cells with tail current amplitude of more than 400 pA and a stable whole-cell membrane resistance of at least 350 MOhm were used. After the control phase the test compounds were applied for 10 min per concentration if not stated differently. All measurements were done at room temperature. Automated patch-clamp recordings and determination of the half-maximal blocking concentration (IC_{50}) of Au1.4MS were performed using the CytoPatch (Cytocentrics Bioscience GmbH) as described previously (33). The inhibitory effect of Au1.4MS on the hERG tail currents was determined after up to 24 min wash-in of Au1.4MS dissolved in EC or after a clear steady-state level of current inhibition was achieved. To activate hERG tail currents the following pulse protocol was used in manual and automated patch-clamp recordings: 0.2 s at –80 mV, 0.2 s at –50 mV, 2 s at +40 mV, and 2 s at –50 mV to elicit hERG tail currents; holding potential was –70 mV; and pulse protocol repetition was every 10 s. Data were recorded and analyzed using the HEKA patchmaster software. Further analysis was performed with Microsoft Excel. The peak amplitude of the hERG tail current was corrected by the value of the leak current determined with the –50-mV pulse before the depolarizing activation pulse.

Docking Simulations. For the docking simulations we use Monte Carlo (MC) simulations (34), using a classical force field, which contains terms for electrostatics, hydrogen bonding, Lennard–Jones potential, and implicit solvent interactions (in a solvent-accessible surface model). Charges for the channel were derived for ambient pH 6.7 and 7.4, using the program pdb2pqr (35, 36), to model the system in the limit of both a fully aqueous and a more neutral environment. The charges for Au1.4MS (12) were derived by density functional theory (DFT) calculations with Turbomole (37). The degrees of freedom are rotation and translation of the rigid bodies and dihedral angle rotations for the single bonds of the ligand. The position of the receptor is kept fixed as a reference and the position of the atoms at the Au_{55} cluster is also kept at their experimental value. Simulations were carried out at room temperature and comprised 200,000 steps in total, sampling both the inner and the outer pore in independent simulations. Each step comprised a displacement and rotation of the particle as well as a reorientation of the internal degrees of freedom of the ligands on the particle.

Animal Tests. All experiments involving genetically modified organisms or animal experimentation were approved by local and state authorities after consulting an Ethics committee appointed by the State of North-Rhine Westfalia in accordance with German Law.

Animals. Nine-week-old male C57BL/6N mice were obtained from a commercial breeder (Charles River Wiga GmbH). Mice were kept in a climate-controlled room (22 °C; 45–54% relative humidity) with a 12-h light/12-h dark cycle.

AuNPs injection. AuNPs were adjusted to the desired dose in 0.9% NaCl and administered at 50 mg/kg body weight through single tail vein injection. Higher doses were not tried, because acute toxicity was observed at >100 mg/kg during initial dose-finding trials. The absence of QT prolongation in the ECG at 50 mg/kg shows that the acute toxicity was not caused by cardiotoxicity. Mice injected with 0.9% NaCl were used as a control group. Each group contained three mice.

ECG measurement. The mouse ECG was measured by the Vevo770 system. The mouse was anesthetized with 2.5% isoflorane and was fixed in the 37 °C prewarmed platform. Electrode gel was applied to the four paws and paws were taped to the ECG electrodes. The signal was acquired by the system from the platform. The ECG waveform was recorded continuously for 2 min. The respiration rate of the mice was under control and maintained between 30 and 70 times per minute during the measurement. The ECG was taken from the mouse before injection and 6 d postinjection.

ACKNOWLEDGMENTS. The authors thank Jan Timper for transmission electron microscopy measurements, Birgit Hahn for support with gold nanoparticle synthesis, Ingrid Rosenkranz for help with the patch-clamp recordings, Gesa Lüdemann for the density functional theory calculations, and Alexander Biewer for support for the docking simulations. This work was supported by the Deutsche Forschungsgemeinschaft (Investigator Grants Si609/9 and Ja562/13), and the Federal Ministry of Education and Research (BMBF) Project "Design of Nanoparticle-Peptide Interactions".

1. Tiwari PM, Vig K, Dennis VA, Singh SR (2011) Functionalized gold nanoparticles and their biomedical applications. *Nanomaterials* 1(1):31–63.
2. Daniel M-C, Astruc D (2004) Gold nanoparticles: Assembly, supramolecular chemistry, quantum-size-related properties, and applications toward biology, catalysis, and nanotechnology. *Chem Rev* 104(1):293–346.
3. Giljohann DA, Mirkin CA (2009) Drivers of biodiagnostic development. *Nature* 462(7272): 461–464.
4. Kim B, et al. (2010) Tuning payload delivery in tumour cylindroids using gold nanoparticles. *Nat Nanotechnol* 5(6):465–472.
5. Popovtzer R, et al. (2008) Targeted gold nanoparticles enable molecular CT imaging of cancer. *Nano Lett* 8(12):4593–4596.
6. Cutler JI, Auyeung E, Mirkin CA (2012) Spherical nucleic acids. *J Am Chem Soc* 134(3): 1376–1391.
7. Pan Y, et al. (2007) Size-dependent cytotoxicity of gold nanoparticles. *Small* 3(11):1941–1949.
8. Pan Y, et al. (2009) Gold nanoparticles of diameter 1.4 nm trigger necrosis by oxidative stress and mitochondrial damage. *Small* 5(18):2067–2076.
9. Pan Y, et al. (2013) High sensitivity real-time analysis of nanoparticles toxicity in green fluorescent protein expressing zebrafish. *Small* 9(6):863–869, 10.1002/smll.2012.

10. Schmid G, Klein N, Korste L, Kreibig U, Schönauer D (1988) Large transition metal clusters-VI. Ligand exchange reactions on $Au_{55}(PPh_3)_{12}Cl_6$-The formation of a water soluble Au_{55} cluster. *Polyhedron* 7:605–608.
11. Krug HF, Wick P (2011) Nanotoxicology: An interdisciplinary challenge. *Angew Chem Int Ed Engl* 50(6):1260–1278.
12. Sanguinetti MC, Tristani-Firouzi M (2006) hERG potassium channels and cardiac arrhythmia. *Nature* 440(7083):463–469.
13. Fermini B, Fossa AA (2003) The impact of drug-induced QT interval prolongation on drug discovery and development. *Nat Rev Drug Discov* 2(6):439–447.
14. Food and Drug Administration (2005) *ICH S7B Guideline of FDA* (Food and Drug Administration, Rockville, MD).
15. Mitcheson JS (2003) Drug binding to HERG channels: Evidence for a 'non-aromatic' binding site for fluvoxamine. *Br J Pharmacol* 139(5):883–884.
16. Kirchner C, et al. (2005) Cytotoxicity of colloidal CdSe and CdSe/ZnS nanoparticles. *Nano Lett* 5(2):331–338.
17. Mitcheson JS, Chen J, Lin M, Culberson C, Sanguinetti MC (2000) A structural basis for drug-induced long QT syndrome. *Proc Natl Acad Sci USA* 97(22):12329–12333.
18. Lees-Miller JP, Duan Y, Teng GQ, Duff HJ (2000) Molecular determinant of high-affinity dofetilide binding to HERG1 expressed in Xenopus oocytes: Involvement of S6 sites. *Mol Pharmacol* 57(2):367–374.
19. Myokai T, Ryu S, Shimizu H, Oiki S (2008) Topological mapping of the asymmetric drug binding to the human ether-à-go-go-related gene product (HERG) potassium channel by use of tandem dimers. *Mol Pharmacol* 73(6):1643–1651.
20. Nanoprobes (2009) The first Gold Nanoparticle X-ray Contrast Agent for in vivo use. Available at www.nanoprobes.com/instructions/Inf1102.html.
21. Schmid G (1985) Developments in transition metal cluster chemistry – the way to large clusters. *Struct Bond* 62:51–85.
22. Wales DJ, et al. The Cambridge Cluster Database. Available at http://www-wales.ch.cam.ac.uk/CCD.html.
23. Long SB, Campbell EB, Mackinnon R (2005) Crystal structure of a mammalian voltage-dependent Shaker family K^+ channel. *Science* 309(5736):897–903.
24. Stary A, et al. (2010) Toward a consensus model of the HERG potassium channel. *ChemMedChem* 5(3):455–467.
25. Staudacher I, et al. (2011) hERG K+ channel-associated cardiac effects of the antidepressant drug desipramine. *Naunyn Schmiedebergs Arch Pharmacol* 383(2):119–139.
26. Casals E, Pfaller T, Duschl A, Oostingh GJ, Puntes V (2010) Time evolution of the nanoparticle protein corona. *ACS Nano* 4(7):3623–3632.
27. Lacerda SH, et al. (2010) Interaction of gold nanoparticles with common human blood proteins. *ACS Nano* 4(1):365–379.
28. Salama G, London B (2007) Mouse models of long QT syndrome. *J Physiol* 578(Pt 1):43–53.
29. Antzelevitch C (2007) Ionic, molecular, and cellular bases of QT-interval prolongation and torsade de pointes. *Europace* 9(Suppl 4):iv4–iv15.
30. Joó F, et al. (1998) (Meta-sulfonatophenyl)diphenylphosphine, sodium salt and its complexes with rhodium(I), ruthenium(II), iridium(I). *Inorg Synth* 32:1–8.
31. Schmid G, et al. (1981) $Au_{55}[P(C_6H_5)_3]_{12}Cl_6$ – ein Goldcluster ungewöhnlicher Größe [Au55[P(C6H5)3]12Cl6 – a gold cluster of unusual size]. *Chem Ber* 114:3634–3642.
32. Negishi Y, et al. (2004) Magic-numbered Au_n clusters protected by glutathione monolayers (n = 18, 21, 25, 28, 32, 39): Isolation and spectroscopic characterization. *JACS* 126:6518–6519.
33. Scheel O, Himmel H, Rascher-Eggstein G, Knott T (2011) Introduction of a modular automated voltage-clamp platform and its correlation with manual human Ether-à-go-go related gene voltage-clamp data. *Assay Drug Dev Technol* 9(6):600–607.
34. Metropolis N, Rosenbluth AW, Rosenbluth MN, Teller AH, Teller E (1953) Equation of state calculations by fast computing machines. *J Chem Phys* 21:1087–1092.
35. Dolinsky TJ, et al. (2007) PDB2PQR: Expanding and upgrading automated preparation of biomolecular structures for molecular simulations. *Nucleic Acids Res* 35(Web Server issue):W522–W525.
36. Dolinsky TJ, Nielsen JE, McCammon JA, Baker NA (2004) PDB2PQR: An automated pipeline for the setup, execution, and analysis of Poisson-Boltzmann electrostatics calculations. *Nucleic Acids Res* 32:W665–W667.
37. Ahlrichs R, Bär M, Häser M, Horn H, Kölmel C (1989) Electronic structure calculations on workstation computers: The program system Turbomole. *Chem Phys Lett* 162(3):165–169.